文章编号：1001-9014(XXXX)XX-0001-10

DOI:10.11972/j.issn.1001-9014.XXXX.XX.001

Design of LEO-LEO Infrared Laser Occultation System for Atmospheric Composition Detection

LIU Yun-Meng[1], HUANG Shuo[1], LI Shi-Zhao[1], GUO Hui-Jun[1], YU Ting[2], WANG Xin[3], LIU Yang[4], CHU Qing[1], CHENG Long[1], DING Lei[1*]

(1. Shanghai Institute of Technical Physics, Chinese Academy of Sciences, Shanghai 200083, China;
2. Shanghai Institute of Optics and Fine Mechanics ,Chinese Academy of Sciences, Shanghai 201800;
3. Institute of Atmospheric Physics, Chinese Academy of Sciences, Beijing 100029, China;
4. Innovation Academy for Microsatellite of Chinese Academy of Sciences, Shanghai 201210, China)

Abstract: Understanding the distribution characteristics of atmospheric components and parameters at different altitudes plays a crucial role in deeply comprehending climate change and addressing climate issues. To meet the detection requirements for vertical profiles of multiple atmospheric components (H_2O, CO_2, CH_4, N_2O, O_3, CO, etc.) and line-of-sight wind speed, this study designs an LEO-LEO infrared laser occultation (LIO) system. For payload design, the laser transmitter employs broadband frequency-locked laser source technology to generate highly stable infrared lasers. The receiver utilizes multi-grating spatial heterodyne spectroscopy (SHS), achieving wide spectral coverage (2-2.5 m) and high spectral resolution (≤0.15 cm^{-1}). For data application and orbit simulation, an Abel transform-based inversion method is proposed to synchronously retrieve atmospheric composition and parameter profiles in the Upper Troposphere and Lower Stratosphere (UTLS). Additionally, a simulated occultation orbit system demonstrates a daily occultation event frequency of up to 61 times, with optimized data acquisition processes for single events.

Key words: LEO-LEO infrared laser occultation, atmospheric components and parameters, spatial heterodyne spectrometer

PACS:

LEO-LEO红外激光掩星大气成分探测系统设计

刘云猛[1], 黄 硕[1], 李世钊[1], 郭慧君[1], 余 婷[2], 王 鑫[3], 刘 洋, 楚 晴[1], 成 龙[1], 丁 雷[1*]

(1. 中国科学院上海技术物理研究所,上海 200083;
2. 中国科学院上海光学精密机械研究所,上海 201800;
3. 中国科学院大气物理研究所,北京 100029,中国科学院微小卫星创新研究院,上海 201210)

摘要:掌握大气成分与要素在不同高度的分布特征,对于深入理解气候变化和应对气候问题具有重要作用。为了满足多大气成分(H_2O、CO_2、CH_4、N_2O、O_3、CO等)和视线风速垂直廓线的探测需求,开展了红外激光掩星探测系统设计。在载荷设计方面,激光发射端设计采用宽谱段频率锁定激光光源技术,制造高稳定性的红外激光;激光接收端设计采用多光栅空间外差光谱探测技术,实现较宽谱段范围、高光谱分辨率探测,光谱范围覆盖2~2.5 μm,光谱分辨率优于0.15 cm^{-1}。在数据应用与轨道仿真方面,基于Abel变换的红外激光掩星反演方法,可实现大气成分与要素廓线在UTLS区域的同步反演;并基于仿真模拟系统进行了掩星轨道设计,经仿真分析计算掩星事件发生频次可达到61次/天,并对单次事件的数据采集过程进行了合理设计规划。

关 键 词:红外激光掩星;大气成分与要素;空间外插光谱仪

中图分类号:TP394.1;TH691.9　　**文献标识码**:A

Received date: 2025-05-16,　　**收稿日期**:2025-05-16,

Foundation items:supported by the National Key Research and Development Program of China (2024YFB3907800).

Biography:LIU YuMeng (1978-), male, Pizhou, master. Research area involves Space photoelectric remote sensing and application technology. E-mail: lym_sitp@163.com.

[*] **Corresponding author**:E-mail: leiding@mail.sitp.ac.cn

Introduction

Research on atmospheric composition is critical for addressing global climate change. Accurate vertical distribution data of atmospheric components are essential alongside total column measurements. Current spaceborne infrared hyperspectral detection technologies can retrieve atmospheric temperature and humidity profiles, playing a significant role in atmospheric research and numerical weather prediction[1-3]. LEO-LEO infrared laser occultation (LIO), a novel active remote sensing technique, enables direct atmospheric profiling with high precision, vertical resolution, global coverage, long-term stability, and all-weather capability, overcoming limitations of traditional satellite observations. LIO requires at least one laser-transmitting satellite (Tx) and one receiving satellite (Rx) for atmospheric observation, as shown in Figure 1. In 2004, the Wegener Center for Climate and Global Change (WEGC) proposed the ACCURATE mission, using microwave and infrared laser occultation between two Low Earth Orbit (LEO) satellites to measure temperature, humidity, pressure, and greenhouse gases. NASA's ATOMMS program (2005) combined GPS-LEO and LEO-LEO occultation[4]. The first ground-based LIO demonstration in 2011 (144 km path, 2.4 km altitude) achieved CO_2 uncertainty of 2% (10-min average) but faced challenges with CH_4 (10 – 15% deviation) due to signal limitations[5]. In 2017, the Chinese Academy of Sciences proposed the CACES mission for LEO-LEO occultation to retrieve atmospheric parameters and gas profiles[6]. By 2019, Li Wendong from the Shanghai Institute of Optics and Fine Mechanics optimized CO_2 detection channels via simulations, achieving a relative random error <0.8%[7]. In 2022, Li Hu et al. from the Shanghai Institute of Technical Physics developed LIO methods for atmospheric temperature and humidity retrieval, demonstrating errors below 1.05 K for temperature and 4% for water vapor number density in the UTLS region [8]. In 2024, Kong Xiangjin et al. from the Changchun Institute of Optics and Fine Mechanics designed hyperspectral imaging optics for occultation-based trace gas detection [9]. These studies collectively provide crucial references for the design and implementation of spaceborne LIO atmospheric detection systems.

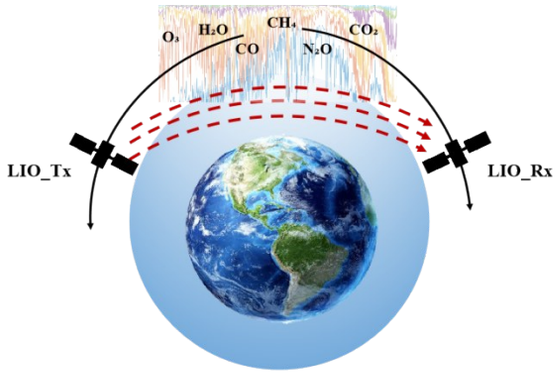

Fig. 1 Schematic of LIOdetection
图 1 红外掩星探测示意图

Since the conceptualization of LIO, relevant research initiatives have been launched both domestically and internationally, yielding notable progress. Table 1 presents a comparative analysis of these global missions [10-11]. No operational in-orbit implementation of LIO missions has been achieved internationally, while domestic research primarily remains at the stage of simulation and theoretical validation[5-6]. This paper conducts a systematic design of payload specifications, data applications, and orbital operations specifically for LIO. The findings establish a foundational basis for atmospheric composition detection via LIO technology.

1 . Scientific requirements and LIO principles

Global climate change and its effective mitigation are among the most critical scientific challenges facing humanity today. Understanding and characterizing the spatiotemporal variations and climatic effects of atmospheric components rely on long-term global atmospheric monitoring, which requires not only accurate total column distributions of atmospheric components but also high vertical-resolution and high-precision observational data of these components and parameters. To address the demand for vertical profile detection of key atmospheric constituents (H_2O, CO_2, CH_4, N_2O, O_3, and CO) in global climate change research, this study investigates space-based infrared laser occultation technology, offering a novel technical approach for probing the vertical

Table. 1 LEO-LEO occultation missions
表 1 LEO-LEO掩星任务

Mission Proposal	Year of Proposal	Agency/Lead Institute	LMO Frequencies (GHz); LIO Freq.	Constellation/Numbers of Satellites
ACCURATE	2005	ESA/WEGC	17.25,20.2,22.6179.0,182.0;SWIR 2-2.5 μm	LMIO constellation,4 LEOs (2Tx-2Rx)
ATOMMS	2007	NSF, NASA/ U. Arizona	Signals near 22 & 183 GHz H_2O vapor, 184 & 195 GHz O_3 lines	ground-based and aircraft-to aircraft occultation demonstrations
CACES	2017	Chinese Academy of Sciences	9.7,13.5 ,17.25,22.6;SWIR 2-2.5 μm	LMIO constellation,4 LEOs (2Tx-2Rx)

structures of multiple atmospheric components and wind speed. The performance requirements aligned with the scientific objectives are detailed in Table 2.

LIO system consists of LEO-LEO satellites equipped with Tx and Rx, respectively. The geometric configuration is illustrated in Figure 2, where α, φ, θ, r_0, and e denote the laser path bending angle, the angle between the two satellites and the Earth's center, the angle between the laser transmission direction and the Earth's center line, the tangent point radius, and the laser transmission direction, respectively [7].

At specific geometric positions, the transmitter emits two pulsed laser beams with closely spaced wavelengths along the same atmospheric path. One laser wavelength (λ_{on}) is tuned to the absorption peak of the target gas, where absorption is strong, while the other wavelength (λ_{off}) is positioned at an absorption valley of the target gas, where absorption is negligible, serving as a reference. After traversing the atmosphere and undergoing absorption and scattering, both λ_{on} and λ_{off} signals reach Rx . The photodetector at Rx converts the optical signals into electrical signals, whose amplitudes depend on atmospheric absorption, scattering properties, and laser wavelength. The resulting electrical signals thus encode the distribution and concentration of absorbing and scattering species. According to the Lambert-Beer law, assuming the incident light intensity is I_0, the outgoing light intensity I can be expressed as:

$$I = I_0 e^{-\tau} \tag{1}$$

Where τ is the optical depth of the atmospheric constituent. During the laser occultation detection process, the laser beam traverses different atmospheric altitude layers, encountering significant differences in temperature and pressure along the observation path. Using the principle of differential absorption detection, the absorbed optical depth $\tau(h)$ can be calculated:

$$\tau(h) = -ln\frac{I_R(\lambda_{on})I_T(\lambda_{off})}{I_T(\lambda_{on})I_R(\lambda_{off})} \tag{2}$$

Where I_R and I_T represent the light intensity at the receiver and transmitter, respectively. Since f λ_{on} and λ_{off} are spectrally close, absorption and scattering effects from other gases and aerosols are nearly identical at both wavelengths. Differential processing cancels out these broadband atmospheric effects, significantly enhancing measurement accuracy. As the satellites move relative to each other, occultation events enable near-vertical scanning of the atmosphere (top-down or bottom-up), yielding vertical profiles for precise characterization of atmo-

Table. 2 LIO system requirements
表 2 红外激光掩星指标需求

Element	Requirement
Wavelength range	2 - 2. 5 μm
Detectable components	≥6 species (H_2O, CO_2, CH_4, N_2O, O_3, and CO)with line-of-sight wind speed
Signal-to-noise ratio (SNR)	≥500
Noise-equivalent power (NEP)	≤ 4×10^{-13}W
Laser frequency stability	≤ 1×10^{-10}/20s
Altitude coverage	5-60 km
Vertical resolution	0. 5-1 km
Daily occultation events	≥50

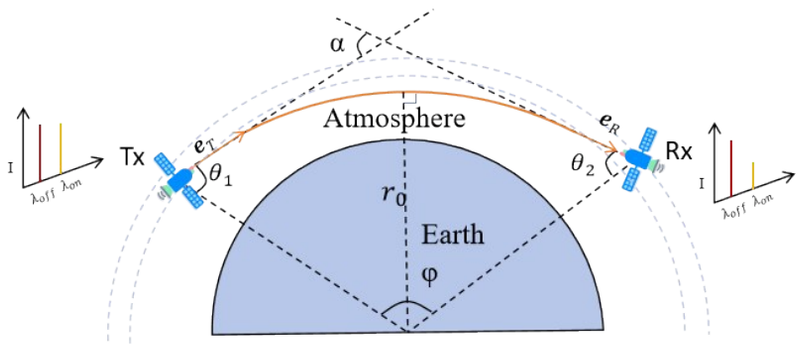

Figure. 2 Schematic of the LIO geometric configuration.
图 2 红外掩星几何结构示意图

spheric composition.

The total loss from transmitter to receiver comprises three components: geometric propagation loss , atmospheric loss and Rx optical system loss[7].

$$P_R = P_T \cdot K \cdot \tau \cdot \eta \tag{3}$$

In the formula, P_R and P_T represent the received power and transmitted power, respectively, K denotes the spatial propagation loss:

$$K = \frac{2(d_r^2/4)\pi}{(D \cdot (\alpha/2))^2 \pi} \tag{4}$$

where D is the Tx-Rx distance, α is the beam divergence angle, d_r is the receiver front-mirror diameter, and the factor 2 accounts for the Gaussian intensity distribution near the optical axis. Atmospheric loss τ includes gas absorption, aerosol absorption, and Rayleigh scattering. Optical loss η encompasses receiver inefficiencies. These losses are modeled to evaluate parameters such as channel selection, laser energy, received power, and SNR[7].

2 System design

2.1 Payload design

The payload of LIO system comprises two critical components: Tx and Rx. Tx emits multiple laser wavelengths that traverse the Earth's atmospheric limb to reach the receiver. Tx employs SHS to measure the intensity of the incident laser wavelengths. Tx is designed modularly to emit multiple laser wavelengths, covering the required spectral range for measurements. Rx utilizes an interferometric spectrometer to measure the intensity of incoming wavelengths. This design enables different laser modules to share a common opto-mechanical system, enhancing cost-effectiveness and flexibility. Each Rx module is configured to cover a specific spectral range centered on a selected wavelength, while multiple transmitter modules can be flexibly tuned to meet detection requirements for various atmospheric components, thereby improving adaptability across diverse application scenarios. Absorption and reference wavelengths are selected based on atmospheric absorption characteristics. Using a wavelength multiplexing method, each receiver module covers a defined spectral range around its central wavelength. Individual receiver modules are dedicated to distinct spectral regions. Increasing the number of measurement wavelengths within these ranges does not necessitate additional receiver modules. The outputs of laser modules are externally combined into a single transmitting telescope, while all receiver modules share a common receiving telescope.

2.2 Channel design

Based on the detection requirements for gas components and parameters, the 2 – 2.5 μm spectral range is selected for infrared laser occultation due to its minimal scattered solar radiation at the receiver optics and the presence of suitable spectral absorption lines. These lines enable high-sensitivity detection of all target atmospheric components and parameters (e. g. , H_2O, CO_2, CH_4, N_2O, O_3, CO, and wind speed) in the Upper Troposphere and Lower Stratosphere (UTLS) region. Frequencies are optimized for maximum sensitivity to target gases in the UTLS while maintaining minimal sensitivity to interfering species, ensuring robust detection performance . Differential transmission measurements require both IR laser absorption and reference signals. [16]The atmospheric radiative transfer model is used to simulate spectra at different vertical altitudes to obtain simulated images of atmospheric transmittance (Figure 4), enabling the screening of detection spectra for atmospheric constituents. The absorption wavelength is selected near the center of the target gas absorption line. Excessive absorption reduces SNR, while insufficient absorption weakens the differential signal. The reference wavelength is positioned at an absorption valley of the target gas. To ensure similar non-target gas absorption characteristics between the two wavelengths, their separation is constrained to within 0.5%[4]. This differential approach effectively corrects broadband effects (e. g. , defocusing, residual scattering, absorption background, aerosol extinction, and scintillation), isolating the target gas absorption signature. The designed detection spectra (Table 3) spans 2 – 2.5 μm, covering absorption lines and their reference counterparts for H_2O, CO_2, CH_4, N_2O, O_3, CO, and wind speed.

2.3 Design of laser light source

The Tx employs a broadband frequency-locked laser source with ultrahigh stability. As schematically illustrated in Figure 5, the system comprises three core modules: (1) Short-wave infrared (SWIR) high-power single-fre-

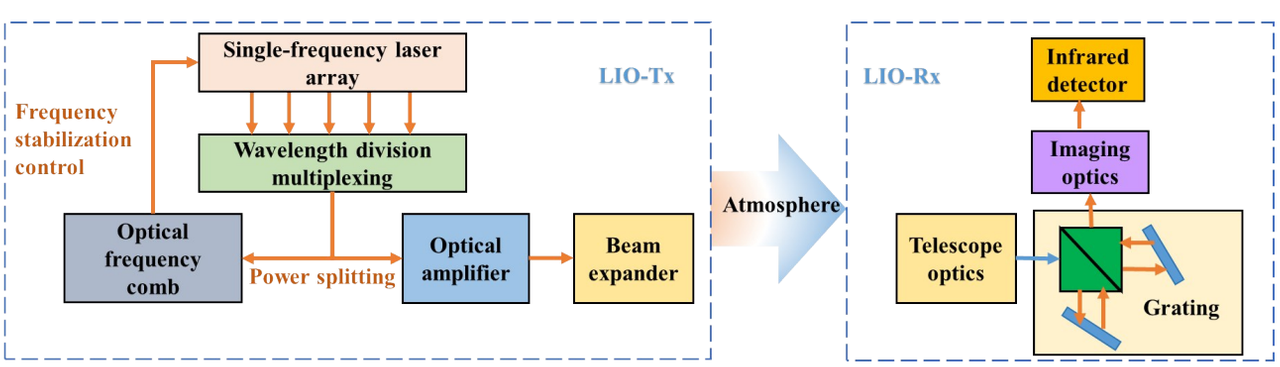

Fig. 3 LIO system payload design
图3 红外激光掩星载荷系统设计

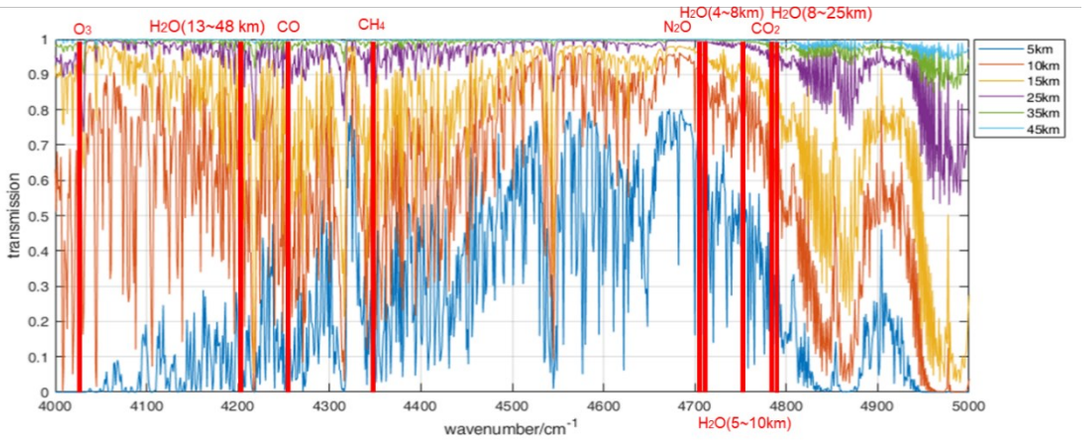

Fig. 4 LIO spectral simulation
图 4 红外激光掩星探测光谱仿真

Table. 3 Required set of LIO channels
表 3 掩星光谱通道设计

Channel ID	Wavenumber (cm^{-1})	Wavelength(μm)	Channel Utility
I01	4029.110	2.4819	O_3(absorption)
I02	4037.21	2.4770	O_3(reference)
I03	4204.840	2.3782	H_2O-1(absorption)~13-48 km(altitude)
I04	4227.07	2.3657	H_2O, CO(reference)
I05	4248.318	2.3539	CO(absorption)
I06	4322.93	2.3133	CH_4(reference)
I07	4344.164	2.3019	CH_4(absorption)
I08	4710.341	2.1230	N_2O(absorption)
I09	4731.03	2.1137	N_2O, H_2O(reference)
I10	4733.045	2.1128	H_2O-4(absorption)~4-8 km(altitude)
I11	4747.055	2.1066	H_2O-3(absorption)~5-10km(altitude)
I12	4767.037	2.09775	wind retrieval
I13	4767.045	2.09773	wind retrieval
I14	4770.15	2.0964	CO_2, H_2O, wind(reference)
I15	4771.621	2.0957	CO_2(absorption)
I16	4775.803	2.0939	H_2O-2(absorption)~8-25 km(altitude)

quency tunable seed source; (2) Miniaturized broadband optical frequency comb (OFC) locking unit; (3) Single-frequency laser power amplifier. This integrated design achieves compact packaging, high reliability, and exceptional stability, delivering >1 W output power per channel with frequency stability : 1×10^{-10} / 20s.

For the broadband miniaturized optical frequency comb locking technology, the key challenge to address is the all-fiber or all-waveguide design of each subunit of the optical frequency comb. This involves developing a miniaturized, broadband (2-2.5 μm) optical frequency comb based on an all-polarization-maintaining (PM) fiber figure-9 cavity mode-locked source combined with nonlinear waveguide self-referencing technology. Furthermore, the single-frequency laser seed source is locked onto the comb lines of the optical frequency comb to achieve broadband frequency stability locking.

Research areas related to the optical frequency comb include:

(1) All-PM fiber figure-9 cavity mode-locking technology: Utilizing the design of all-PM fibers and fiber devices to realize a highly stable, highly compact optical frequency comb mode-locked seed source.

(2) All-fiber and waveguide-based self-referencing technology: To obtain a high signal-to-noise ratio (SNR) carrier-envelope offset (CEO) frequency. The spectral range of the erbium-doped fiber optical frequency comb is extended to the 2.0-2.5 μm band.

(3) High-bandwidth phase-locked loop (PLL) technology: Using ultra-stable crystal oscillators as the microwave frequency reference, and implementing long-term locking of the optical frequency comb's repetition frequency and CEO frequency through PID feedback control based on a phase-locked loop.

Regarding the short-wave infrared high-power single-frequency tunable laser source and its power enhancement, the development focuses on a watt-level broadband laser source based on Cr:ZnS/ZnSe materials. This incorporates broadband tunable technology, linewidth control technology, and power amplification technology, with the output locked onto the comb lines of the optical frequency comb.

2.4 Design of multi-grating SHS

SHS offers advantages such as high optical throughput, high spectral resolution, no moving parts, and compact structure, aligning well with the development trends of miniaturization, modularization, and standardization in remote sensing[12-15]. The optical system of the spatial heterodyne spectrometer primarily consists of three components: a front collimation system, an interferometer assembly, and an imaging system. For the SHS, the front collimation system provides parallel light within a specific field of view to the interferometer assembly and positions the exit pupil of the collimation system onto the dispersive grating within the interferometer. After spatial interference modulation by the interferometer assembly, the resulting interference pattern is ultimately imaged onto the detector via the imaging system. By adopting a multi-grating SHS design, the spectral range is expanded significantly without compromising spectral resolution. This resolves the traditional trade-off between spectral coverage and resolution, achieving the broad spectral range and high spectral resolution required for atmospheric composition detection.

According to the multi-channel design requirements for atmospheric composition detection, a three-channel interferometer (SWIR1-3) structure is adopted. Spectral resolution of each band can be described by[12]

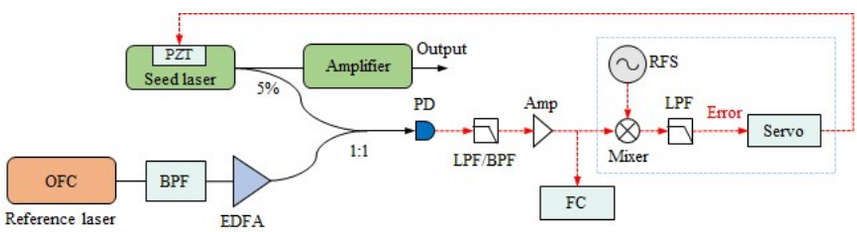

Fig. 5 The laser light source composition
图 5 激光光源组成图

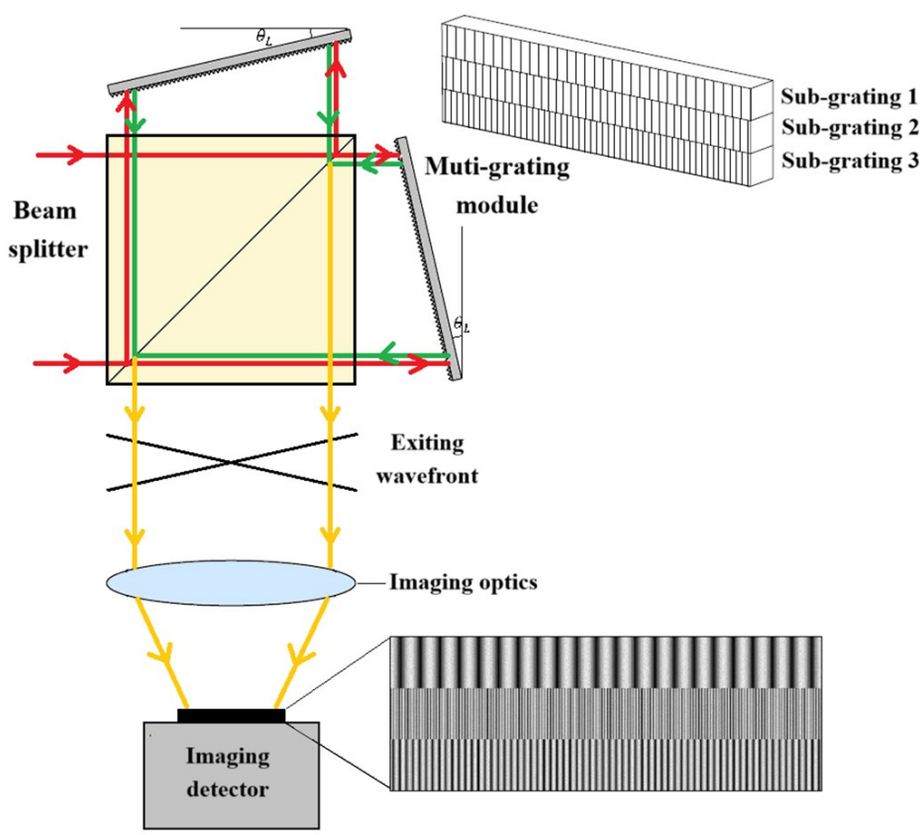

Fig. 6 Structure of the SHS of LIO payload
图 6 多光栅空间外差光谱仪组成示意图

$$\delta\sigma = \frac{1}{4W\sin\theta_L} \tag{5}$$

which is determined by the grating width (W) and the Littrow angle (θ_L). The maximum resolvable bandwidth of each spectral band can be described by

$$\Delta\sigma = \frac{N}{2} \times \delta\sigma = \frac{N}{8W\sin\theta_L} \tag{6}$$

This bandwidth is related to the number of detector pixels and the spectral resolution of each band. The spectral resolution and maximum resolvable bandwidth are equal for all bands.

From the grating equation:

$$2d\sin\theta_L = m\lambda_L \tag{7}$$

it follows that once the Littrow angle is determined, the grating constant corresponds uniquely to the Littrow wavelength. The comprehensive optical parameters of the system are summarized in the table below:

Optical simulations were conducted to model the image plane patterns under simultaneous incidence of all wavelengths(fig 7). The fringes observed in the three regions of the detector result from the linear superposition of interference patterns generated by incident light of all wavelengths within their respective channels. The simulation results confirm the rationality and feasibility of the optical design structure and parameters.

The spatial heterodyne spectrometer captures interference fringe images using a two-dimensional array detector. Data processing methods—including image preprocessing, interferogram processing, and Fourier transform are required to transform the interference signal into a spectral signal. The use of a two-dimensional array detector allows the acquisition of multiple interferograms within the same channel, utilizing multiple sampling to improve the signal-to-noise ratio. The interferograms undergo preprocessing steps such as spike removal and apodization. Subsequently, a Fourier transform is applied to obtain the spectral signal. Radiometric calibration is then performed to correct the signal and derive the spectral intensity. Finally, the optical thickness of atmospheric components is retrieved through spectral differencing calculations.

2.5 Multi-component and parameter vertical synchronous retrieval method

Based on the principle of multi-channel infrared differential absorption, the LIO detector transmits pairs of infrared laser wavelengths—strongly absorbed (λ_{on}) and weakly absorbed (λ_{off}) by target gases. The receiver captures both laser signals attenuated by the atmosphere, enabling vertical synchronous retrieval of multiple atmospheric components and parameters.

(1) Retrieval of Volume Mixing Ratio Profiles Using Atmospheric Absorption Information

The energy or amplitude of the laser signal received by the infrared laser occultation system is closely related to atmospheric transmittance. Atmospheric transmittance (Tr) is defined as the ratio of the attenuated signal intensity (I) to the unattenuated intensity (I_0) at the top of the atmosphere:

$$T_r = \frac{I}{I_0} = e^{-\tau} \tag{8}$$

The optical thickness (τ) of an atmospheric component represents the integral of the absorption coefficient (k) along the observation path:

Table. 4 Multi-Grating SHS optical parameter
表 4 多光栅光谱仪光学参数

	B1	B2	B3
Channel ID	I01-I02	I03-I07	I08-I16
Wavenumber (cm^{-1})	4029. 171-4037. 142	4204. 861-4248. 269; 4322. 829-4344. 237	4710. 316-4775. 777
grating width (mm)	54	54	54
Spectral resolution (cm^{-1})	0. 1354	0. 1354	0. 1354
Effective pixels of the detector	1280×140	1280×140	1280×140

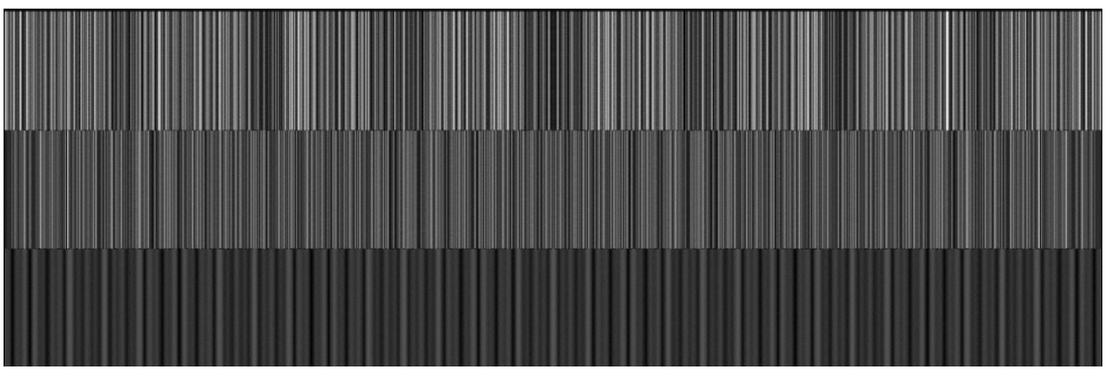

Fig. 7 SHS Interference simulation diagram
图 7 空间外差光谱仪干涉仿真图

$$\tau = \int_{Tx}^{Rx} k ds \tag{9}$$

Signal intensity I is proportional to the square of the amplitude A. Transmittance can thus be derived from the amplitude:

$$T_r(a) = -20[\log A(a) - \log A_{ds}(a)] \tag{10}$$

where a denotes the impact parameter, and A_{ds} accounts for defocusing and divergence effects. Using Abel integral transform, the absorption coefficient is derived from transmittance:

$$k = \frac{1}{\pi}\frac{da}{dr}\Big|_{a=a_0} \int_{a_0}^{\infty} \frac{d\ln T_r}{da}\frac{1}{(a^2 - a_0^2)}da \tag{11}$$

Under the spherical symmetry assumption, challenges such as weak singularities at the lower limit and initialization at the upper limit may introduce errors during discretization and inversion. Corrections are applied to refine the absorption coefficient. Finally, the absorption coefficient is converted to volume mixing ratio V (ppmv) via the gas state equation:

$$V(z) = 10^6 R\frac{k(z)}{\sigma(z)}\frac{T(z)}{p(z)} \tag{12}$$

where T is temperature (K), p is atmospheric pressure (Pa), R is the universal gas constant (8.3145 $J\cdot K^{-1}\cdot mol^{-1}$), and$\sigma$is the absorption cross-section (m^2/mol) of the target gas, calculated using the HITRAN2020 molecular absorption database.

Retrieving multi-component volume mixing ratio profiles involves two steps: Firstly, deriving individual gas profiles using the equations above. Secondly., synthesizing multiple profiles while minimizing cross-component interference through optimized retrieval sequencing, ultimately achieving synchronized multi-component retrievals.

(2) Retrieval of vertical line-of-Sight wind speed profiles using doppler shift

The Doppler shift is employed to retrieve line-of-sight horizontal wind speeds along the transmitter-receiver link. The Doppler frequency shift (Δf_w) is expressed as:

$$\Delta f_w = -f_0 v_{\parallel}/c \tag{13}$$

where$v_{\parallel}$is the line-of-sight wind speed, c is the speed of light in a vacuum, and f0 is the signal frequency in the Earth-fixed reference frame.

Assuming constant wind speed along each occultation path, the Doppler shift is derived from differential absorption measurements of closely spaced laser signals:

$$\Delta f_w = \frac{(Tr_{w1} - Tr_{w2}) - (Tr_{w1}^0 - Tr_{w2}^0)}{\left(dTr/df\right)_{w1} - \left(dTr/df\right)_{w2}} \tag{14}$$

Where Tr_{w1}andTr_{w2} are the transmittances of two wind channels, while Tr_{w1}^0 and Tr_{w2}^0 are baseline transmittances under static atmospheric conditions. Solving these equations yields:

$$v_{\parallel} = -\frac{\left[(Tr_{w1} - Tr_{w2}) - (Tr_{w1}^0 - Tr_{w2}^0)\right]\cdot c}{\left[\left(dTr/df\right)_{w1} - \left(dTr/df\right)_{w2}\right]\cdot f_0} \tag{15}$$

2.6 Orbit simulation-based occultation event planning

The LIO orbit simulation system was employed for orbit design and occultation event analysis. A Sun-synchronous orbit was selected to achieve ≥50 occultation events per day, with the following design principles:

(1) Stable satellite link geometry: Identical orbit types for transmitting and receiving satellites were chosen to ensure consistent orbital plane drift rates.

(2) For global coverage, the sub-satellite points of the signal intersections between the transmitting and receiving satellites must vary. In the longitudinal direction, full coverage is readily achievable due to Earth's rotation and nodal precession of the orbital planes. However, in the latitudinal direction, achieving global coverage requires differing orbital periods for the transmitting and receiving satellites, implying placement at different orbital altitudes (differing semi-major axes).

(3) Subject to constraints including the number of occultation events (≥50), ground track drift per event (≤ 50 km), and occultation duration (≥10 s), an orbit design featuring closely spaced transmitter and receiver altitudes was developed. Simulation analysis led to the selection of 500 km and 550 km as the optimal orbital heights.

For a single-transmitter-single-receiver configuration, the average occultation duration is ~12 s, yielding 61 daily events. The simulated occultation event distribution is shown in Figure 8.

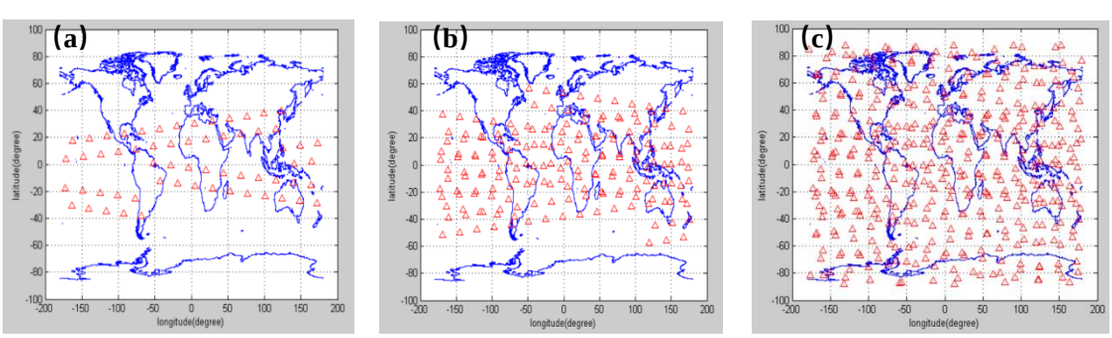

Figure. 8 Distribution of occultation events: (a)distribution of LIO envents in a day(61 times); (b)distribution of LIO envents in 3 days(182 times); (c)distribution of LIO envents in a week(424 times)

图 8 掩星事件分布:(1)一天掩星事件分布(61次);(2)三天掩星事件分布(182次);(3)一周掩星事件分布(424次)

Task planning for occultation data acquisition: Frequency stabilization for 16 channels completed before acquisition. Infrared laser pulses emitted at four time points (2 ms duration each), with background collection (2 ms) and readout (0.5 ms) per pulse, forming a 20 ms cycle. The acquisition process is illustrated in Figure 9.

Observation efficiency analysis: Annual occultation opportunities (N_y) scale with satellite numbers (m: transmitters, n: receivers) as:

N_y=22133×m×n

Annual observation counts for various constellations are listed in Table 5.

Table. 5 Annual occultation observation opportunities for constellation configurations
表 5 一年掩星星座观测次数规划

Constellation	Annual Observations
1Tx—1Rx	22133
1Tx—2Rx	44265
1Tx—3Rx	66397
2Tx—2Rx	88527
3Tx—3Rx	199190

3 Conclusions

A space-based infrared laser occultation system was designed to meet vertical profiling demands for atmospheric components (H_2O, CO_2, CH_4, N_2O, O_3, CO) and wind speed. Key innovations include:

1. LIO-Rx employs a multi-grating spectrometer design that conserves payload space while achieving hyperspectral detection with 0.135 cm^{-1} resolution across the 2 – 2.5 μm spectral range.

2. A broad -spectra frequency-locked laser source technology is adopted for the illumination system, featuring miniaturized design to cover short-wave infrared (SWIR) bands with exceptional stability (10^{-10}/20s).

3. A channel-multiplexed differential detection methodology is implemented to enable multi-frequency atmospheric vertical sounding, significantly enhancing detection efficiency and vertical resolution.

This system design provides critical technical support for future in-orbit occultation missions, advancing global atmospheric monitoring capabilities.

	Module1		Module2					Module3				Module4				
	I01	I02	I06	I07	I04	I03	I05	I09	I08	I10	I11	I14	I12	I13	I15	I16
T1	1	1	1	1				1	1			1	1			
T2					1	1		1		1		1		1		
T3					1		1	1			1	1			1	
T4												1				1

Figure. 9 Design of occultation event acquisition process
图 9 掩星时间采集过程设计

References

[1] SONG Ci, YIN Qiu. Evaluation on vertical space characteristics of atmospheric water vapor and ozone for FY-4A GIIRS data sounding [J]. J. Infrared Millim. Waves, 2021, 40(4): 539~546.
(宋慈,尹球. FY-4A GIIRS数据探测大气水汽和臭氧的垂直空间特性评估[J].红外与毫米波学报),2021,40(4):539~546.

[2] CHEN Ren, GAO Cong, WU Xiao-Wei, ZHOU Si-Yu, HUA Jian-Wen, DING Lei. Application of FY-4 atmospheric vertical sounder in weather forecast [J]. J. Infrared Millim. Waves, 2019, 38 (3): 285~289.
(陈仁,高聪,吴晓唯,周思宇,华建文,丁雷.(英)风云四号大气垂直探测仪在气象预报中应用[J].红外与毫米波学报),2019,38(3):285~289.

[3] HUANG Shuo, GU Ming-Jian, HU Yong, YANG Tian-Hang, SHAO Chun-Yuan, ZHANG Chun-Ming. Nonlinear response correction method for on-orbit data of FY-3E hyperspectral infrared atmospheric sounder II [J]. J. Infrared Millim. Waves, 2024, 43 (1): 118~125.
(黄硕,顾明剑,胡勇,杨天杭,邵春沅,张春明.红外高光谱大气探测仪(FY-3E/HIRAS-II)在轨数据非线性校正方法[J].红外与毫米波学报),2024,43(1):118~125.

[4] KIRCHENGAST G. ACCURATE-Climate benchmark profiling of greenhouse gases and thermo-dynamic variables and wind from space, ESA Earth Explorer Opportunity Mission EE8 Proposal, Scientific Report 36-2010[R]. Graz, Austria: Wegener Center Verlag, 2010.

[5] Proschek V., Kirchengast G., Schweitzer S., et al., 2015. Retrieval and validation of carbon dioxide, methane and water vapor for the Canary Islands IR-laser occultation experiment. Atmos. Measure. Techniq. 8, 3315 – 3336.

[6] Zhang Z H, Wang X, Lv D R.Progress of temperature and water vapor profiles detected by LEO-LEO microwave occultation [J].Journal of Telemetry, Tracking and Command, 2022, 43(01): 1-12.
(张志华,王鑫,吕达仁.LEO-LEO微波掩星探测温度和水汽廓线研究进展[J].遥测遥控),2022,43(01):1-12.

[7] Li W D, Liu J Q, Zhu Y D, et al. LEO-LEO Infrared Laser Occultation Tecnique to Measure Atmospheric Carbon Dioxide Concentration. [J]Chinese Journal of Lasers, 2019, 46(08): 263-269.
(李文冬,刘继桥,朱亚丹,等.LEO-LEO红外激光掩星CO2浓度测量技术研究[J].中国激光),2019,46(08):263-269.

[8] Kong X J, Li B, Li S S, et al. Optical system design of hyperspectral imaging spectrometer for trace gas occultation detection [J]. Chinese Optics, 2024, 17(03): 661-673.
(孔相金,李博,李寒霜,等.痕量气体掩星探测高光谱成像光谱仪光学系统设计[J].中国光学(中英文)),2024,17(03):661-673.

[9] Li H, Wang J Y and Hong G L. 2022. Retrieval method and simulation of UTLS temperature and water vapor by laser occultation [J]. National Remote Sensing Bulletin, 26(10): 1935-1945.
(李虎,王建宇,洪光烈.激光掩星探测大气UTLS温度和水汽的方法及仿真[J].遥感学报),2022,26(10):1935-1945.

[10] Shi J C, Lü D, Wang Y, et al.Recent Progress of Earth Science Satellite Missions in China [J].Chinese Journal of Space Science, 2022, 42(4): 12.DOI: 10.11728/cjss2022.04.yg21.

[11] Liu C L, Kirchengast G, Syndergaard S, et al. A review of low Earth orbit occultation using microwave and infrared-laser signals for monitoring the atmosphere and climate [J]. Advances in Space Research, no. 12 (2017): 2776-2811.

[12] Ye S , Fang Y H, Hong J, et al.System design of spatial heterodyne spectrometer [J]. Optics and Precision Engineering, 2006, (06): 959-964.
(叶松,方勇华,洪津,等.空间外差光谱仪系统设计[J].光学精密工程),2006,(06):959-964.

[13] Smith B W, Harlander J. Imaging spatial heterodyne spectroscopy: theory and practice [C]//SPIE, 1999, 3698:925-931.

[14] Watchorn S, Roesle F L, Harlander J, et al. Development of the spatial heterodyne spectrometer for VUV remote sensing of the interstellar medium[C]//SPIE, 2001, 4498: 284-295.

[15] Harlander J, Roesler F L, Cardon J G, et al. SHIMMER: a spatial heterodyne spectrometer for remote sensing of Earth′smiddle atmosphere [J]. Applied Optics, 2002, 41 (7): 1343-1352.

[16] Proschek V, Kirchengast G, Schweitzer S, et al. ACCURATE: greenhouse gas profiles retrieval from combined IR-laser and microwave occultation measurements [C] // EGU General Assembly Conference 2010, May 2-7, 2010, Vienna , Austria.[S.1: s.n], 2010: 14352